Flash Droughts in the Wake of Landfalling Atlantic Tropical Cyclones

Vasubandhu Misra[1], Tyler Sherrod[1], and Jayasankar C B[1]

[1]Florida State University

November 21, 2022

Abstract

Using a novel but a proven strategy to detect Flash Droughts (FDs), we identified four cases out of 30 (˜13%) landfalling Atlantic TCs over the period of 2000-2018 Atlantic hurricane seasons that were associated with FD events in their wake. In all four instances of these FD events, the principal causes were found to be the rapid reduction in precipitation and warming of the surface temperature despite the moderate to weak anomalously wet soil prevalent in the wake of the landfalling TC. These FD cases assume significance because they occurred in southeastern US, which is primarily energy limited for evapotranspiration in the summer. Furthermore, all four cases of FD occurred coincidentally with a more widespread, neighboring drought near the landfall region, which suggests that these FD extend these large-scale droughts from the exacerbated conditions in the wake of the landfalling TC.

Hosted file

`essoar.10511910.1.docx` available at https://authorea.com/users/530080/articles/597272-flash-droughts-in-the-wake-of-landfalling-atlantic-tropical-cyclones

Flash Droughts in the Wake of Landfalling Atlantic Tropical Cyclones

Vasubandhu Misra[1, 2, 3, #], Tyler Sherrod[1, 2] and C. B. Jayasankar[2, 3]

[1]Department of Earth, Ocean and Atmospheric Science, Florida State University, Tallahassee, Florida, U. S. A.

[2]Center for Ocean-Atmospheric Prediction Studies, Florida State University, Tallahassee, Florida, U. S. A.

[3]Florida Climate Institute, Florida State University, Tallahassee, Florida, U. S. A.

#Corresponding Author: vmisra@fsu.edu

Key points:

1. The new, simplified flash drought index correctly identifies several well-known, documented flash drought events in Continental US.
2. Flash droughts are exacerbated by rapid increase in surface temperature and decline in precipitation in the wake of the Atlantic TC
3. Flash droughts from Atlantic TCs are found to be extension of neighboring large-scale drought but occurring at a rapid rate

Abstract

Using a novel but a proven strategy to detect Flash Droughts (FDs), we identified four cases out of 30 (~13%) landfalling Atlantic TCs over the period of 2000-2018 Atlantic hurricane seasons that were associated with FD events in their wake. In all four instances of these FD events, the principal causes were found to be the rapid reduction in precipitation and warming of the surface temperature despite the moderate to weak anomalously wet soil prevalent in the wake of the landfalling TC. These FD cases assume significance because they occurred in southeastern US, which is primarily energy limited for evapotranspiration in the summer. Furthermore, all four cases of FD occurred coincidentally with a more widespread, neighboring drought near the landfall region, which suggests that these FD extend these large-scale droughts from the exacerbated conditions in the wake of the landfalling TC.

Plain Language Summary

The work discusses an underreported threat of droughts in the wake of Atlantic Tropical Cyclones (TCs). Most landfalling TCs are associated with threats of wind damage and flooding while the potential of droughts in the wake of Atlantic TCs is not discussed prior to this study. Flash Droughts (FDs) are identified when there is a rapid deterioration of "drought like" conditions that usually manifest in some unique combination of declining precipitation, soil moisture, and increasing surface temperature. We find that FDs occur in 4 of the 30 landfalling Atlantic TCs between 2000 and 2018, in the post landfall period of less than 1 to 12 weeks. Many of these FDs are an extension of

a pre-existing, developing large-scale drought near the landfall region that is exacerbated by subsidence in the wake of the landfalling TC. These FD events associated with landfalling TC in Louisiana and Florida are significant because in these regions' during the hurricane season evapotranspiration is not limited by surface moisture but by downwelling surface energy from the persistence of low cloud cover. This threat of FD though relatively uncommon from landfalling Atlantic TC does pose an additional challenge to combat their threat.

1 Introduction

Flash Drought (FD) events are characterized by rapid intensification of drought that initially begin as a meteorological drought that transitions to agricultural drought (Otkin et al. 2013, 2018 [hereafter OTK13 and OTK18]). Such rapid manifestation of droughts can severely impact ecosystems, agricultural productivity, manifest as heat waves, cause increased risk of wildfire development, deplete water resources, and reduce air quality, causing a threat to public health and economic loss (OTK13; Mo and Lettenmaier 2015; Christian et al. 2019).

The diversity in the definition of FDs is significant (OTK18). For example, some define FDs by their duration (e.g., Mo and Lettenmaier 2015, 2016). Other studies argue that rate of intensification of drought rather than duration defines a FD (OTK18). There is also diversity in the choice of the variables in detecting FDs ranging from using soil moisture index to estimate wilting and field capacity metric (Hunt et al. 2009) to standard precipitation index (Hunter et al. 2014), standardized precipitation-evapotranspiration index (Christian et al. 2019) and evapotranspiration stress index (OTK13). Furthermore, many of these earlier studies depend on complex surface energy balance or land surface models to obtain measures of evaporative stress. Therefore, we were motivated to introduce a simpler methodology for detection of FDs that can be easily computed from observed or analyzed variables, like surface temperature, precipitation, and soil moisture. Although, it should be stressed that the soil moisture dataset used in this study is a product of reanalysis and land-surface models. It should be mentioned that there is also diversity in the duration of the diagnosed FD events based on the definitions ranging from within a week (Mo and Lettenmaier 2015, 2016) to a month (Christian et al. 2019) to several months (OTK18).

Several studies suggest that the United States is one of the most affected countries by both floods and droughts (Villarini et al. 2011; Retchless et al. 2014; Zhou et al. 2018). However, in the post-landfall period the likelihood of sustained dry and warm period can cause human misery, fatalities, and lead to collateral losses. In many of these cases, the heat stress from high wet bulb temperatures in days after landfall become life threatening, as was evident from the tragic deaths from heat stress during the post-Hurricane Irma (2017) period in Hollywood, Florida (Berman et al. 2017).

There is evidence to suggest that TCs influence the large-scale environment in their wake. For example, Sobel and Camargo (2005) find that the large-scale environment in the primary region of TC activity, lagging the accumulated cy-

clone energy by about two weeks, becomes far less conducive for cyclogenesis from reduction of SST and precipitable water, and with increase in outgoing longwave radiation. Some of these conditions can also lead to rapid intensification of drought. In fact, Scoccimarro et al. (2020) show that the western Pacific typhoon-induced drying of the Maritime Continent (manifesting as moisture flux divergence) results in the onset of their dry season. In this study we investigate the occurrence of FDs from landfalling Atlantic TCs from 2000 to 2018. In the following section the methodology to detect FDs is described. The results are presented in Section 3, followed by a discussion and conclusions in Section 4. The data used in the study is described in the supplementary section (S1).

2 Methodology to diagnose flash droughts

We compute the daily cumulative anomaly (D_k) of soil moisture, precipitation, and temperature, separately, as:

$$D_k = \sum_{k=n}^{m} \overline{d}_k^{'} \text{ - - - - - - - - - - - - - - - (1)}$$

Where, overbar denotes area average over a 500km radius (this choice is not critical and is just used for illustration here) around a single grid point in the middle of an already identified FD event. Incidentally, in the case of landfalling TCs a radius of 500km is found to be an optimal radius for encompassing the TC induced precipitation shield (Jiang and Zipser 2010; Zhou, Y. et al. 2018). Further,

$$D_k \in \begin{cases} S_k \\ P_k \\ T_k \end{cases} \text{ and } \overline{d}_k^{'} \in \begin{cases} \overline{s}_k^{'} \\ \overline{p}_k^{'} \\ \overline{t}_k^{'} \end{cases}$$

Where, S_k, P_k, T_k are daily cumulative anomaly of soil moisture, precipitation, and temperature, respectively; $\overline{d}^{'}$ is the corresponding daily area averaged anomalies, k is the time index in days starting from the n^{th} to the m^{th} day. The daily anomaly, $d_k^{'}$ is given by:

$$d_k^{'} = \overline{d}_k - \overline{\overline{d}}_k \text{ - - - - - - - - - - - - (2)}$$

Where, $\overline{d}_k$ are daily area averaged soil moisture or temperature or precipitation and $\overline{\overline{d}}_k$ represents the corresponding climatology for day k, respectively. The daily cumulative anomaly (D_k) curves are then normalized by their standard deviation (σ_D) to make them unitless:

$$\widehat{D}_k = \frac{D_k}{\sigma_D} \text{ - - - - - - - - - - - - (3)}$$

Where,

$$\widehat{D}_k \in \begin{cases} \widehat{S}_k \\ \widehat{P}_k \\ \widehat{T}_k \end{cases},$$

Then a consolidated, normalized cumulative anomaly curve, which will be called the Consolidated Drought Index [CDI] curve ($\widehat{C}_k$) is computed as:

$$\widehat{C}_k = \widehat{S}_k + \widehat{P}_k + \left(-\widehat{T}_k\right) - - - - - - - - - - - - - (4)$$

The idea of CDI curve is to isolate the conditions of the FD characterized by rapid decrease in soil moisture and precipitation and an increase in surface temperature or some combination of their anomalies. Therefore, the FD is recognized by the rate of change of CDI (≤ -0.05/day) over at least an eight week period. The threshold of -0.05/day was obtained empirically from examining the efficacy of the methodology on several of the previously studied FDs.

Incidentally, in the case of landfalling TCs a radius of 500km is found to be an optimal radius for encompassing the TC induced precipitation shield (Jiang and Zipser 2010; Lee et al. 2010; Khouakhi et al. 2017; Zhou, Y. et al. 2018). We further require that the FD must manifest within a month of the landfall.

In the following section we describe the results by first verifying the methodology of detecting FDs from CDI on past, documented FD events in the CONUS not connected to any TC landfall. Subsequently, the FD events associated with Atlantic TC landfalls are presented.

4 Results

a) Verification of the Flash Drought Events in Continental US

We verify our FD detection methodology by examining an iconic FD event over the Midwestern United States, in the summer of 2012 (OTK18). Fig. 1a shows the 8-week change in the drought category of the United States Drought Monitor (USDM) ending on July 24, 2012. The FD is diagnosed by a three to five category increase in drought severity over the 8-week period, as per the USDM maps (OTK18; Fig. 1a). OTK18 argue that such a change in the drought category in the USDM map satisfies the conditions for detecting FD which requires that the index first represent drought like conditions and then signify its rapid intensification. The cumulative soil moisture anomaly, area averaged around a radius of 500km centered over St. Louis, Missouri is shown in Fig. 1b. The choice of St. Louis as the center of the 500km radius circle is chosen posteriorly from the analysis of this event in OTK18, which indicates St. Louis to be in the center of the severity of this FD event (e.g., OTK18). Furthermore, the start of the cumulative anomaly curve from April 15, 2012, in Fig. 1b is also based on the earlier analysis of this FD event in OTK18 that documented the precipitous increase in drought severity over the 8-week period

ending on July 24, 2012. We advanced the CDI curve further by 6 weeks earlier to the start of the 8-week period ending on July 24, 2012, to be able to objectively diagnose the start of the FD event. It may be noted that the potential period of FD is far more apparent in the daily cumulative anomaly curve of the soil moisture when there is a steep decline from early May to September (Fig. 1b). In contrast, the daily timeseries of soil moisture in Fig. 1b indicate significant high frequency variability as well as a sharp decline from early May to August (Fig. 1b). Similarly, the corresponding curves of precipitation (Fig. 1c) and surface temperature (Fig. 1d) yet again confirm that the steep decline in precipitation (Fig. 1c) and steep increase in temperature (Fig. 1d) over the period of the FD are more apparent in their respective daily cumulative anomaly curves than their daily timeseries. In Fig. 1e we have plotted the corresponding normalized cumulative anomaly curves of precipitation, soil moisture, temperature, and the CDI. The start and end of the FD period is marked by the steep decline in the CDI curve, which starts from May 01, 2012 and ends on August 15, 2012. It is interesting to note that the CDI curve in Fig. 1e shows the FD period far more clearly than the remaining three other curves in the graph with its steep slope of -0.06 day^{-1}.

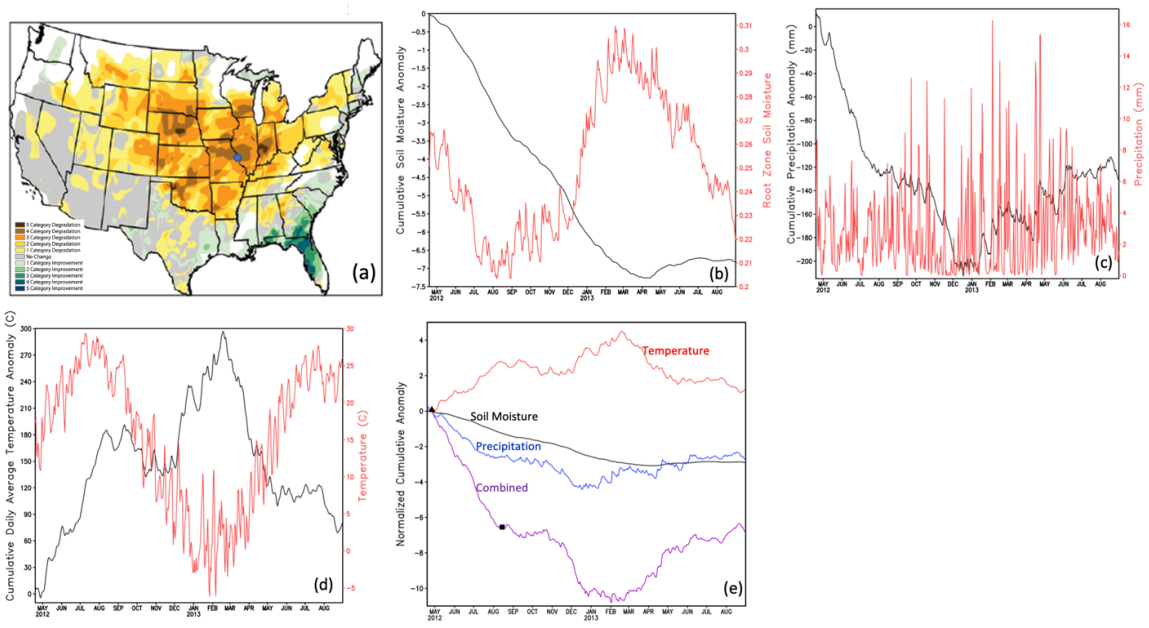

Figure 1: a) FD centered around St. Louis, Missouri (blue dot), showing the 8-week change in the USDM drought category ending on July 24, 2012 (from OTK18). The corresponding area averaged time series at 500km radius centered over St. Louis, Missouri of daily b) cumulative soil moisture anomaly (black line) and soil moisture (red line), c) cumulative precipitation anomaly (mm;

black line) and precipitation (mm day^{-1}; red line), and d) cumulative surface temperature anomaly (black line) and surface temperature (°C; red line). e) The corresponding normalized daily cumulative anomalies of temperature, soil moisture, precipitation, and the CDI curves. The start and end of the FD in Fig. 1e are marked by the black solid triangle (01 May 2012) and square (15 August 2012), respectively. The gradient of the CDI over the FD period from (e) is -0.06 day^{-1}.

Figs. 2a, b, c, and d show the maps of the summation of the daily cumulative soil moisture, precipitation, surface temperature anomalies and the corresponding CDI over the period of the diagnosed FD, which illustrates the spatial extent of the FD. The spatial patterns of the accumulated soil moisture anomalies over the FD period in Fig. 2a resemble to some extent the spatial pattern of the change in drought category from USDM in Fig. 1a. This FD fingerprint is also apparent in the accumulated precipitation anomaly, which is negative, over a broad region around St. Louis, Missouri (Fig. 2b). Similarly, the accumulated anomalies of temperature in Fig. 2c show that the largest warming anomalies are stretched over a wide area around St. Louis, Missouri. Finally, the spatial map of the cumulative anomalies of the CDI in Fig. 2d show uniformly, negative value across US except in the southeast and northwest region. However, the regions of high temporal correlations of the CDI in Fig. 1e with the corresponding timeseries of CDI at all other grid points indicate that a smaller subset of this region (hatching) show a precipitous decrease in the CDI as in Fig. 1e. Therefore, the hatched region in Fig. 2d suggest a measure of the spatial extent of the FD of 2012, centered around St. Louis. Although the centroid and start date of the FD event was seemingly "cherry picked" in this example, FD events can be objectively detected from the methodology as CDI is computed at every grid point over CONUS and every day of the year so that the slope of the rate of change of CDI over at least an 8-week period could be routinely examined. In fact, the initial area averaging around a 500km radius would be unwarranted if the mission is to find FD events and not verify the efficacy of the methodology.

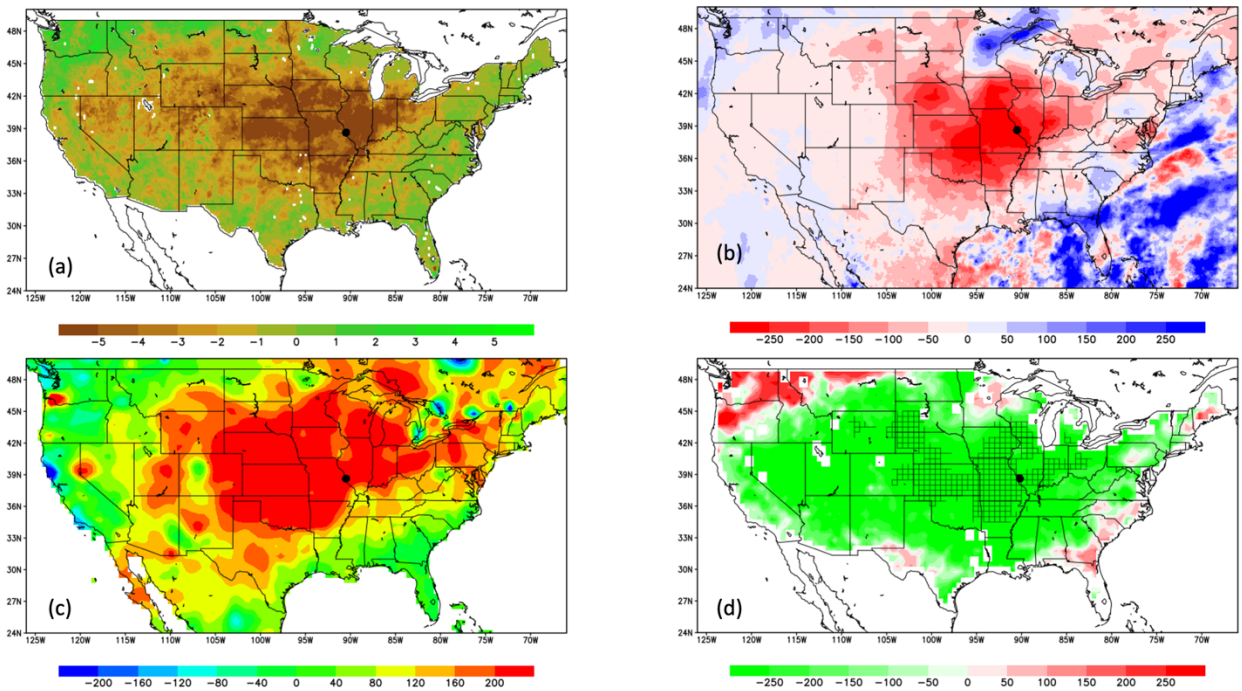

Figure 2: The map of the daily cumulative a) soil moisture, b) precipitation, c) surface temperature, and d) CDI for the FD event centered over St. Louis in 2012 (see Fig. 1a). The daily anomalies are summed over the period of the FD diagnosed in Figure 1e. The hatching in (d) indicates significant correlation (at 1% significance level) of the evolution of the CDI with its corresponding evolution over a 500km radius region around St. Louis indicated in Fig. (1e). The black dot in each of the panels indicate the location of St. Louis, Missouri.

Four other separate cases of FD diagnosed by the National Drought Mitigation Center have been reviewed using the FD detection methodology proposed here (in the supplementary material section S2). In each of these cases the efficacy of the methodology is similarly demonstrated.

b) Flash drought events associated with Atlantic landfalling Tropical Cyclones

We examined all landfalling Atlantic TC's from 2000-2018 in the continental US, of which we were able to identify 4 distinct events that produced FDs post landfall. As in the previous case, the timeseries of all the three variables and the CDI averaged around a radius of 500km from the point of landfall is plotted in Fig. 3 for these four cases of landfalling TCs. The start and end date of the FD are indicated in the timeseries of the CDI for all cases in Fig. 3. The slope of the CDI computed over the period of the FD for Humberto is -0.06 day^{-1} (Fig. 3a), Isaac is -0.07 day^{-1} (Fig. 3b), Matthew is -0.09 day^{-1} (Fig. 3c), and

Harvey is -0.05 day^{-1} (Fig. 3d). These slopes are comparable to the previous cases discussed in Sections 2b and S2.

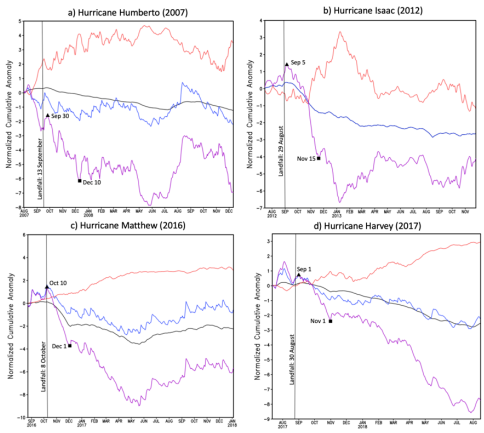

Figure 3: The area averaged time series of the normalized cumulative anomalies of daily soil moisture (black line), precipitation (blue line), surface temperature (red line), and CDI (purple line) for the landfalling case of a) Hurricane Humberto of 2007, b) Hurricane Isaac of 2012 (soil moisture and precipitation lines are indistinguishable), c) Hurricane Matthew of 2016, and d) Hurricane Harvey of 2017. The area average of the time series is conducted over a radius of 500km around the point of landfall. The start and end of the FD are marked by the black solid triangle and square, respectively.

Hurricane Humberto (2007) after passing High Island, Texas moved northeastward toward southwestern Louisiana and became a tropical depression near Alexandria, Louisiana (late on 13 September) before it dissipated over Central Mississippi (Fig. 4a; see Section S3 for life histories of these TCs). In this instance, the FD was diagnosed on September 30 (Fig. 3a), over two weeks from the time the TC made landfall. But we regard this FD to be associated with the landfall of Humberto because the decline in precipitation, the rise in surface temperature, and the gradual decline in soil moisture started to occur soon after landfall of the hurricane, which contributed to the onset of this FD that ended on 10 December (Fig. 3a).

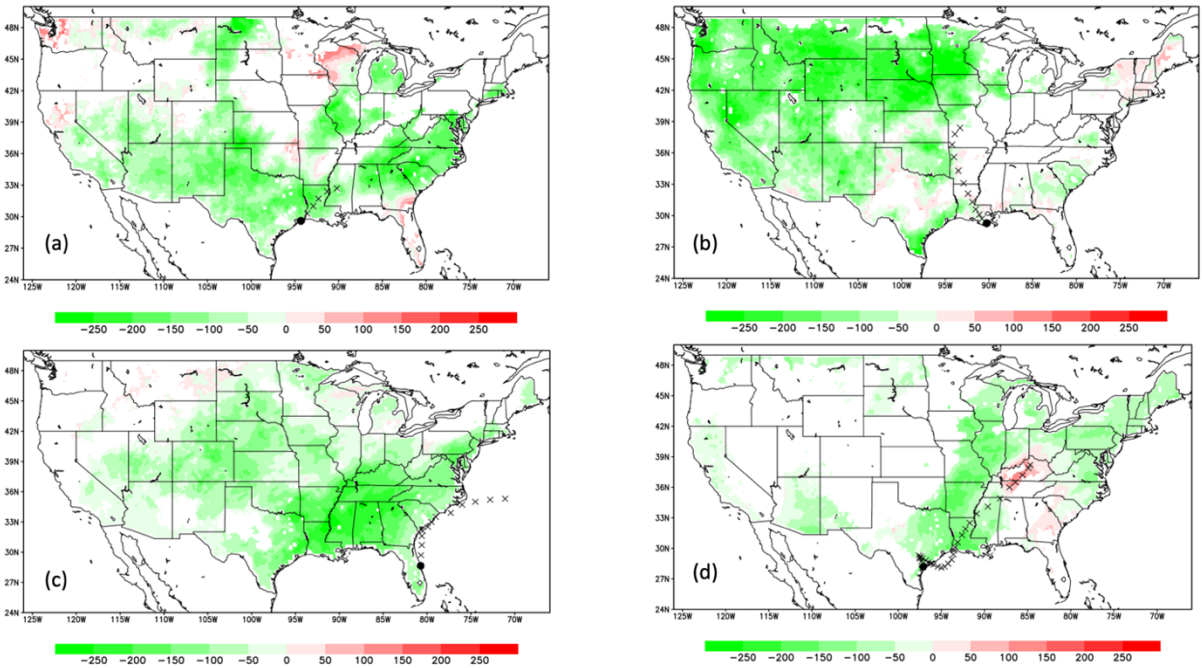

Figure 4: The map of the normalized, daily cumulative anomalies of the CDI for the FD events associated with the landfall of Hurricanes a) Humberto of 2007, b) Isaac of 2012, c) Matthew of 2016, and d) Harvey of 2017. The daily CDI are summed over the period of the FD as indicated in Figure 3. The black dot in each of the panels indicate the location of the landfall of the hurricane. The cross marks indicate the track of the hurricane after its landfall at 6-hour interval from the best track. All shaded values in (d) indicate significant correlation with the evolution of the corresponding CDI curve in Fig. 3 at 95% confidence interval according to t-test.

Hurricane Isaac of 2012 made a second landfall at Port Fourchon, Louisiana around 0800 UTC 29 August (Berg 2013). The onset of the FD associated with this hurricane landfall was diagnosed as 5 September, five days after landfall (Fig. 3b), signaled by comparable decrease in rainfall and soil moisture after landfall. The steep rise in surface temperature however occurs far later, in mid-November, which leads to prolonged duration of the FD that ends on 15 November (Fig. 3b).

Hurricane Matthew (2016) skirted the coast of Florida (Cape Canaveral; Fig. 4c). The diagnosis of the onset of FD around Cape Canaveral occurred on 10 October (Fig. 3c), two days after. The relatively steep decline in precipitation and soil moisture and a gradual increase in surface temperature in the wake of the passage of Hurricane Matthew led to the onset of the FD, manifesting in the sharp decline of the CDI (Fig. 3c).

We observe in the case of Hurricane Harvey (2017), which made landfall in Cameron, southwestern Louisiana on 30 August (Fig. 4d), the onset of FD occurred soon after on September 1 and lasted until November 1 (Fig. 3d). This period of FD was characterized by gradual increase in surface temperature, decline in precipitation and a gradual decrease in soil moisture (Fig. 3d).

The corresponding spatial pattern of these FDs as represented by the values of the CDI over the period of the diagnosed FD is shown in Fig. 4. It is very apparent from these cases that the FD as associated with the landfall of the TC is part of a larger scale drought that stretches far beyond the point of landfall. It is as though, the wake of the landfalling TC was the "last straw that broke the Camel's back" in initiating the FD at the point of landfall. The subsidence in the wake of the landfalling TC (Fig. 5) exacerbates and accelerates the advancing drought over the landfall region. The large-scale subsidence in the wake of the landfalling TC stabilizes and warms the atmospheric column while also reducing the mixing in the boundary layer leading to rising surface temperature and reduced precipitation.

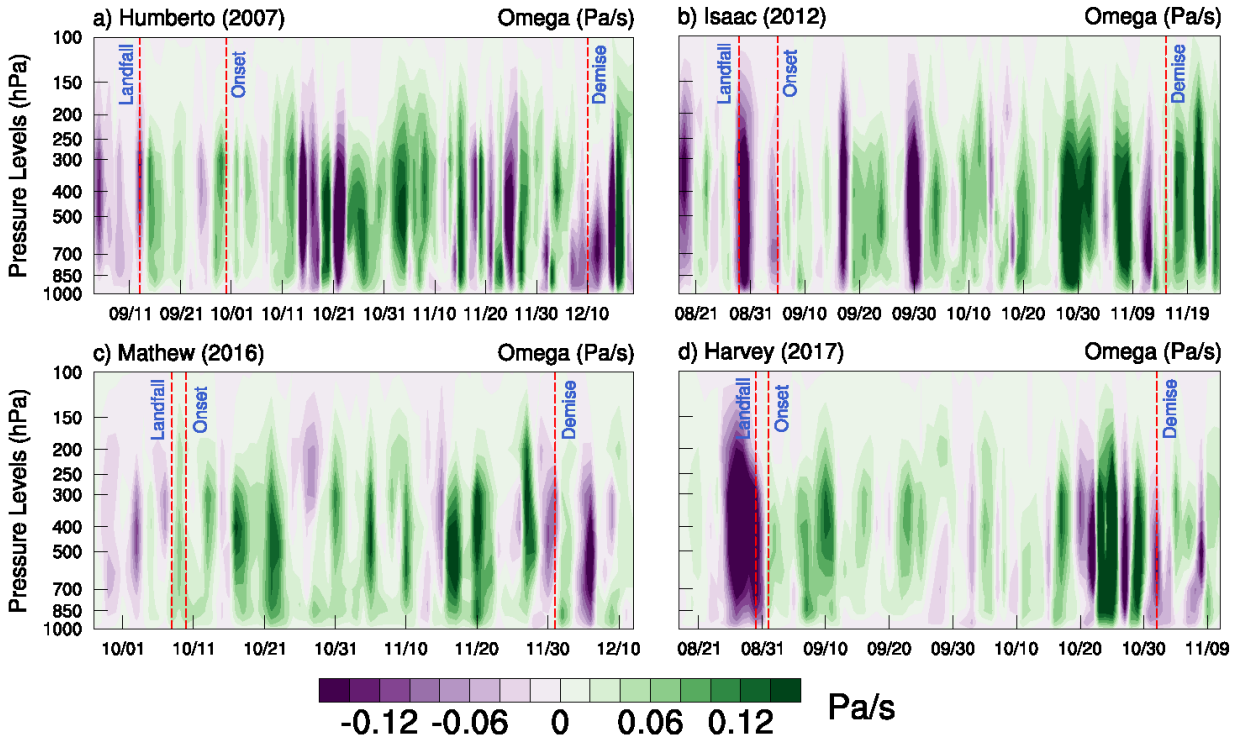

Figure 5: The vertical profiles of omega (Pa/s) area averaged at 500km radius around the landfall point of a) Hurricane Humberto (2007), b) Hurricane Isaac (2012), c) Hurricane Mathew (2016), and d) Hurricane Harvey (2017). The

corresponding dates of landfall, onset, and demise of the diagnosed FD are marked on the x-axis of each panel.

In all these four landfalling TCs, the soil moisture anomaly over the period of the FD is not significant at the point of its landfall (Fig. FS5). The summation of the normalized, daily cumulative anomalies of the soil moisture over the diagnosed FD period around the landfall point in all four cases are positive, suggesting that the soil was anomalously wet, albeit slightly (Fig. FS5). This would seem somewhat obvious given the amount of rainfall from these landfalling TCs and associated storm surge that would have moistened/saturated the soil. However, the corresponding summation of the normalized, daily cumulative anomalies of precipitation over the period of the FD around the landfall point of the TC are well below zero (Fig. FS6). In fact, the dry anomalies in Fig. FS6 nearly track the TC after landfall in all four cases. Similarly, the summation of the normalized, cumulative surface temperature values over the period of the FD are above zero in all four cases (Fig. FS7). These figures suggest that the lack of precipitation and the increasing of surface temperature in the wake of these landfalling TCs leads to the increase in evaporative stress, that leads to the diagnosis of the FD.

5 Discussion and Conclusions

The verification of the well-known FDs from our methodology suggests its efficacy. This methodology is an alternative to existing methods for diagnosing FD with the advantage that we don't require a sophisticated land surface/energy balance model and is based on some easily available variables at daily interval. The threshold for the slope of the rate of change of CDI to be ≤ -0.05/ day over at least an eight-week period to diagnose FD from our methodology is empirical. Additionally, we require the FD to start within a month of the landfall of the TC.

We find that only 13% (4 out of 30) of the Atlantic landfalling TCs in the period between 2000 to 2018 produce FD. In the remaining 26 landfalling Atlantic TCs we observed that either the rate of change of CDI never reached values of ≤ -0.05/day or these slopes were achieved after more than a month after landfall of the TC. This it is not very surprising given that Misra and Dirmeyer (2009) indicate that the eastern half of US, especially the southeastern US where the density of landfalling TCs is the highest in CONUS display a robust seasonal cycle wherein they transition from water limited evapotranspiration regime in winter and spring to energy limited evapotranspiration regime in summer and fall. This is primarily because of the proximity of the region to warm ocean waters in the Gulf of Mexico and tropical Atlantic in the later half of the year that serve as a source of significant boundary layer moisture in the region that manifest in persistent low cloud cover (Jacobs et al. 2002). Therefore, attempting to find periods of rapid increase in evaporative stress (a combination of reduced soil moisture and increasing temperature) in the US Gulf and Atlantic coasts during the hurricane season is likely to be harder than in water limited evapotranspiration regions (e.g., southwestern/midwestern US).

This is also compounded by the fact that we are trying to diagnose FD events in the most unanticipated period of the wake of an extreme wet event like the landfalling Atlantic TC. But the fact we can still isolate at least 4 such cases of 30 landfalling events does make it significant. The four cases of FD in the wake of the Atlantic landfalling TC is also seen to be part of a larger scale drought evolving in the vicinity of the landfall. Therefore, it appears that these FDs associated with landfalling Atlantic TCs may not appear in isolation but in a more widespread region of high evaporative stress.

Acknowledgements

We acknowledge the support from NASA grant 80NSSC19K1199 and 80NSSC22K0595.

Data Availability Statement

Soil moisture data used in the paper is available from: https://catalog.data.gov/dataset/smerge-noah-cci-root-zone-soil-moisture-0-40-cm-l4-daily-0-125-x-0-125-degree-v2-0-smerge-

The CPC Global Temperature data is provided by the NOAA/OAR/ESRL PSL, Boulder, Colorado, USA, from their Web site at: https://psl.noaa.gov/data/gridded/data.cpc.globaltemp.html

The precipitation data used in the paper is available from:

https://psl.noaa.gov/data/gridded/data.cpc.globalprecip.html

References

Berg, R., 2013: Tropical Cyclone Report: Hurricane Isaac. 78 pp. Available from: https://www.nhc.noaa.gov/data/tcr/AL092012_Isaac.pdf.

Berman, M., K. Zezima, and A. C. Davis, 2017: Eight dead after South Florida nursing home's air conditioning fails following Hurricane Irma. Washington Post. Available from: https://www.washingtonpost.com/news/post-nation/wp/2017/09/13/irma-death-toll-rises-as-5-dead-at-south-florida-nursing-home/

Brennan, M. J., R. D. Knabb, M. Mainelli, and T. B. Kimberlain, 2007: Annual summary: Atlantic hurricane season of 2007. Mon. Wea. Rev., 137, 4061-4088.

Chen, M., W. Shi, P. Xie, V. B. S. Silva, V E. Kousky, R. Wayne Higgins, and J. E. Janowiak (2008), Assessing objective techniques for gauge-based analyses of global daily precipitation, J. Geophys. Res., 113, D04110, doi:10.1029/2007JD009132.

Christian, J. I., J. B. Basara, J. A. Otkin, E. D. Hunt, R. A. Wakefield, P. X. Flanagan, and X. Xiao, 2019: A methodology for flash drought identification: application of flash drought frequency across the United States. J. Hydromet., 20, 833-846, https://doi.org/10.1175/JHM-D-18-0198.1.

Hersbach, H., and coauthors, 2020: The ERA5 global reanalysis. Q. Roy. Met. Soc., 146 (730), 1999-2049.

Hoell, A., B. -A. Parker, M. Downey, and coauthors, 2020: Lessons learned from the 2017 flash drought across the U. S. Northern Great Plains and Canadian Prairies. Bull. Amer. Soc., https://doi.org/10.1175/BAMS-D-19-0272.1.

Huffman, G.J., Adler, R.F., Bolvin, D.T., Hsu, K., Kidd, C., Nelkin, E.J., Tan, J. and Xie, P., 2019: Algorithm Theoretical Basis Document (ATBD) for global precipitation climatology project version 3.0 precipitation data. MEaSUREs project, Greenbelt, MD.

Hunt, E., K. G. Hubbard, D. A. Wilhite, T. J. Arkebauer, and A. L. Dutcher, 2009: The development and evaluation of a soil moisture index. *Int. J. Climatol.*, **29**, 747–759, https://doi.org/10.1002/joc.1749.

Jacobs, J. M., S. L. Mergelsberg, A. F. Lopera, and D. A. Meyers, 2002: Evapotranspiration from a wet prairie wetland under drought conditions: Paynes prairie preserve, Florida, USA. Wetlands, 22, 374-385

Jiang, H., and E. J. Zipser, 2010: Contribution of tropical cyclones to the global precipitation from eight seasons of TRMM data: Regional, seasonal, and interannual variations. *J. Climate*, **23**, 1526–1542, https://doi.org/10.1175/2009JCLI3303.1.

Khouakhi, A., G. Villarini, and G. A. Vecchi, 2017: Contribution of tropical cyclones to rainfall at the global scale. *J. Climate*, **30**, 359–372, https://doi.org/10.1175/JCLI-D-16-0298.1.

Landsea, C. W. and J. L. Franklin, 2013: Atlantic Hurricane Database Uncertainty and Presentation of a New Database Format. Mon. Wea. Rev., 141, 3576-3592.

Lee, M.-H., C.-H. Ho, and J.-H. Kim, 2010: Influence of tropical cyclones landfalls on spatiotemporal variations in typhoon season rainfall over South China. *Adv. Atmos. Sci.*, **27**, 443–454, https://doi.org/10.1007/s00376-009-9106-3.

Misra, V. and P. A. Dirmeyer, 2009: Air, sea, and land interactions of the Continental US hydroclimate. J. Hydromet, 10, 353-373.

Mo, K. C., and D. P. Lettenmaier, 2015: Heat wave flash droughts in decline. *Geophys. Res. Lett.*, **42**, 2823–2829, https://doi.org/10.1002/2015GL064018.

Mo, K. C., D. P. Lettenmaier, 2016: Precipitation deficit flash droughts over the United States. *J. Hydrometeor.*, **17**, 1169–1184, https://doi.org/10.1175/JHM-D-15-0158.1.

Otkin, J. A., M. Svoboda, E. D. Hunt, T. W. Ford, M. C. Anderson, C. Hain, and J. B. Basara, 2018: Flash droughts. Bull. Amer. Soc., https://doi.org/10.1175/BAMS-D-17-0149.1.

Otkin, J. A., M. C. Anderson, C. Hain, I. Mladenova, J. Basara, and M. Svoboda, 2013: Examining flash drought development using the thermal infrared based evaporative stress index. *J. Hydrometeor.*, **14**, 1057–1074, https://doi.org/10.1175/JHM-D-12-0144.1.

Powell, M. D., and T. A. Reinhold, 2007: Tropical cyclone destructive potential by integrated kinetic energy. Bull. Amer. Meteor. Soc., 88, 513–526.

Retchless, D.; Frey, N.; Wang, C.M.; Hung, L.S.; Yarnal, B. Climate extremes in the united states: Recent research by physical geographers. *Phys. Geogr.* **2014**, *35*, 3–21.

Rui, H. and J. Dong, 2021: README Document for SMERGE Root-zone Soil Moisture Data Product Version 2.0. Available from: https://hydro1.gesdisc.eosdis.nasa.gov/data/SMERGE/SM

Scoccimarro, E., S. Gualdi, A. Bellucci, D. Peano, A. Cherchi, G. A. Vecchi, and A. Navarra, 2020: The typhoon-induced drying of the Maritime Continent. PNAS. https://doi.org/10.1073/pnas.1915364117.

Sobel, A. and S. J. Camargo, 2005: Influence of Western North Pacific Tropical Cyclones on their large-scale environment. J. Atmos. Sci., 62 (9), 3396-3407

Stewart, S. R., 2017: Tropical Cyclone Report: Hurricane Mathew, 96 pp. Available from https://www.nhc.noaa.gov/data/tcr/AL142016_Matthew.pdf.

Villarini, G.; Smith, J.A.; Baeck, M.L.; Krajewski, W.F. Examining flood frequency distributions in the midwest US. *J. Am. Water Resour. Assoc.* **2011**, *47*, 447–463.

Xie, P., A. Yatagai, M. Chen, T. Hayasaka, Y. Fukushima, C. Liu, and S. Yang (2007), A gauge-based analysis of daily precipitation over East Asia, J. Hydrometeorol., 8, 607. 626.

Zhou, Q, G. Leng, and J. Peng, 2018: Recent changes in the occurrences and damages of floods and droughts in the United States, *Water* 10, no. 9: 1109. https://doi.org/10.3390/w10091109.

Zhou, Y., C. Matyas, H. Li, and J. Tang, 2018: "Conditions associated with rain field size for tropical cyclones landfalling over the Eastern United States". Atmos. Res., 214, doi:10.1016/j.atmosres.2018.08.019.

Supplementary Material

Flash Droughts in the Wake of Landfalling Atlantic Tropical Cyclones

Vasubandhu Misra[1, 2, 3, #], Tyler Sherrod[1, 2, 3] and C. B. Jayasankar[2, 3]

[1]Department of Earth, Ocean and Atmospheric Science, Florida State University, Tallahassee, Florida, U.SA.

[2]Center for Ocean-Atmospheric Prediction Studies, Florida State University, Tallahassee, Florida, U.SA.

[3]Florida Climate Institute, Florida State University, Tallahassee, Florida, U. S. A.

S1: Description of data used in the study

In this study, we use daily root-zone soil moisture, surface temperature, and precipitation to diagnose flash drought. For soil moisture, we use the Soil MERGE (SMERGE; doi:10.5067/PAVQY1KHTMUT) root zone (0-40cm) soil moisture data. The SMERGE product is developed by merging North American Land Data Assimilation version 2 with satellite-based moisture retrievals to produce 0.125° gridded, daily root zone soil moisture for the Continental United States (CONUS; Rui and Dong 2021). For temperature, we use NOAA's Climate Prediction Center gridded, daily, global, land surface temperature (Xie et al. 2007 and Chen et al. 2008) data available from 1979 to the present at 0.5° grid resolution. For precipitation, we use NASA's IMERG Final Run gridded, daily, global, precipitation (Huffman et al. 2019) data available from June 2000 to the present at 0.1° grid resolution. Finally, we use the upper air vertical velocity (omega field) from fifth generation ECMWF atmospheric reanalysis (ERA5, Hersbach et al. 2020). The TC fixes to determine the landfall region and its track post landfall was obtained from HURDAT2 (Landsea and Franklin 2013).

S2: Examples of well-known Flash Droughts

Four other examples of flash droughts occurring in the CONUS and reported in earlier studies are verified with the proposed methodology here. These flash droughts were identified originally by the US Drought Monitor. These examples are shown to demonstrate the efficacy of the methodology introduced in the paper on some of the iconic flash drought events. The flash drought events are initially diagnosed over a 500 km radius around locations previously identified in other studies using the cumulative anomaly curve of the drought index (see main text). Then the maps of the normalized cumulative, soil moisture, temperature, precipitation, and the Consolidated Drought Index (CDI) map are plotted to illustrate the spatial extent of the flash drought. The accumulation of these variables is done over the period of the flash drought initially diagnosed from the timeseries of the drought index illustrated in Panel (a) of each figure.

Fig. FS1a shows the time series evolution of the cumulative anomaly curve of the drought index for 500 km radius centered around Des Moines, Iowa, which detected a flash drought between 07 May 2012 to 15 August 2012 (reported in Otkin et al. 2013). The corresponding maps of the accumulated anomalies of soil moisture (Fig. FS1b), precipitation (Fig. FS1c), surface temperature (Fig. FS1d), and the CDI (Fig. FS1e) illustrate the spatial extent of the flash drought.

This flash drought event over Des Moines overlaps with that of St. Louis and therefore the spatial maps shown in Figs. 2a-d and Figs. FS1b-e appear very similar. The slope of the CDI in Fig. FS1e is 0.06 day^{-1}, which is like that detected for St. Louis in Fig. 1e.

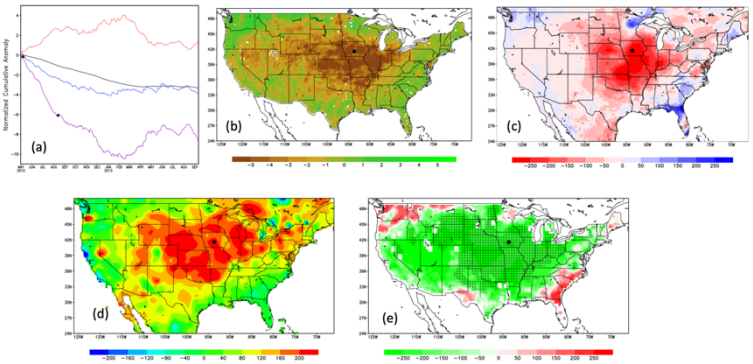

Figure FS1: (a) Normalized daily cumulative anomaly curves of temperature, soil moisture, precipitation, and the drought index computed over an area of 500 km radius centered around Des Moines, Iowa. The start (07 May 2012) and end (15 August 2012) of the flash drought period is indicated by a triangle and a square, respectively. The gradient of the drought index over the flash drought period from (a) is 0.06 day^{-1}. The corresponding cumulative b) soil moisture, c) precipitation, d) surface temperature and e) drought index anomalies over the period of the diagnosed flash drought from (a) with the black dot marking Des Moines, Iowa. The hatching in (e) indicates significant correlation (at 1% significance level) of the evolution of the drought index with its corresponding evolution over a 500km radius region around Des Moines indicated in (a).

The next case of flash drought reviewed is over Glasgow, Montana (Fig. FS2; reported in Hoell et al. 2020). Here, the gradient of the CDI over the flash drought period of 20 May 2017 to 03 August 2017 is 0.07 day^{-1}. The spatial extent of the flash drought event indicated by the hatched area in Fig. FS2e shows a similar decrease in the cumulative anomalies of soil moisture (Fig. FS2b) and precipitation (Fig. FS2c) and an increase in the cumulative anomalies of temperature (Fig. FS2d).

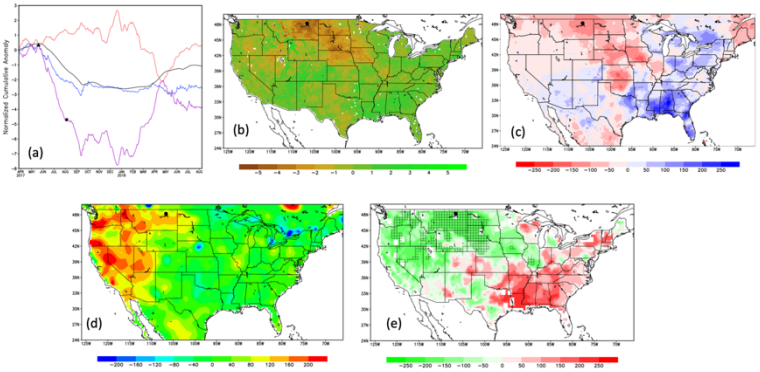

Figure FS2: (a) Normalized daily cumulative anomaly curves of temperature, soil moisture, precipitation, and the drought index computed over an area of 500 km radius centered around

Glasgow, Montana. The start (20 May 2017) and end (03 August 2017) of the flash drought period is indicated by a triangle and a square, respectively. The gradient of the drought index over the flash drought period from (a) is 0.07 day^{-1}. The corresponding cumulative b) soil moisture, c) precipitation, d) surface temperature and e) drought index anomalies over the period of the diagnosed flash drought from (a) with the black dot marking Glasgow, Montana. The hatching in (e) indicates significant correlation (at 1% significance level) of the evolution of the drought index with its corresponding evolution over a 500km radius region around Glasgow indicated in (a).

For further illustration of the methodology in detecting flash drought events recognized by the National Drought Mitigation Center, we have analyzed the flash drought event over Richmond, Indiana (18 April 2007 to 01 July 2007; Fig. FS3; reported in Otkin et al. 2013) and Tifton, Georgia (03 October 2016 to 27 November 2016; Fig. FS4; identified in Christian et al. 2019). Both these cases show similar evolution and detection of the flash drought events as the previous events (e.g., St. Louis, Glasgow, Des Moines).

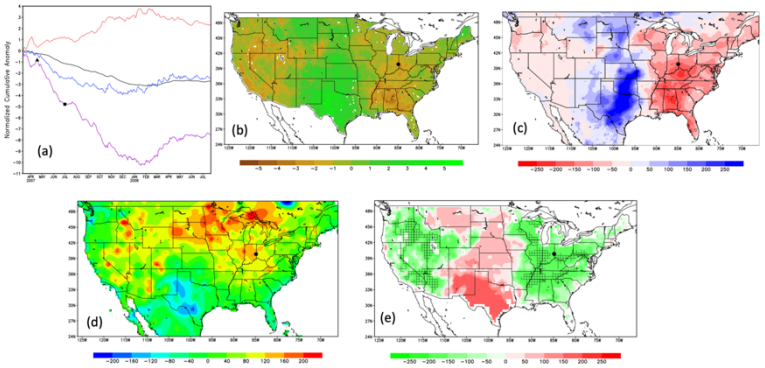

Figure FS3: (a) Normalized daily cumulative anomaly curves of temperature, soil moisture, precipitation, and the drought index computed over an area of 500 km radius centered around Richmond, Indiana. The start (18 April 2007) and end (01 July 2007) of the flash drought period is indicated by a triangle and a square, respectively. The gradient of the drought index over the flash drought period from (a) is 0.05 day^{-1}. The corresponding cumulative b) soil moisture, c) precipitation, d) surface temperature and e) drought index anomalies over the period of the diagnosed flash drought from (a) with the black dot marking Richmond, Indiana. The hatching in (e) indicates significant correlation (at 1% significance level) of the evolution of the drought index with its corresponding evolution over a 500km radius region around Richmond indicated in (a).

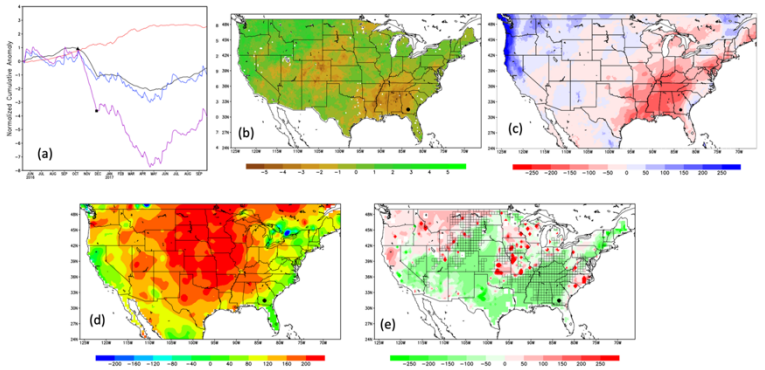

Figure FS4: (a) Normalized daily cumulative anomaly curves of temperature, soil moisture, precipitation, and the drought index computed over an area of 500 km radius centered around Tifton, Georgia. The start (03 October 2016) and end (27 November 2016) of the flash drought period is indicated by a triangle and a square, respectively. The gradient of the drought index over the flash drought period from (a) is 0.07 day^{-1}. The corresponding cumulative b) soil moisture, c) precipitation, d) surface temperature and e) drought index anomalies over the period of the diagnosed flash drought from (a) with the black dot marking Tifton, Georgia. The hatching in (e) indicates significant correlation (at 1% significance level) of the evolution of the drought index with its corresponding evolution over a 500km radius region around Tifton indicated in (a).

These results suggest that our proposed methodology can detect these well-known flash drought events over CONUS. Additionally, the methodology shows the period of the flash drought objectively with its start and end date marked by the ends of the slope of the rate of change of CDI, which is $\sim \geq |0.05|$/day.

S3: Brief life histories of the four Atlantic TCs that produced flash droughts

(i) Hurricane Humberto (2007)

Hurricane Humberto was a Category 1 hurricane evolved from a depression that formed 194 km (105 n mi) south of Galveston, Texas around 0900 UTC 12 September, which became a tropical storm by 1200 UTC 12 September 2007. Humberto became a hurricane (with ~80kt winds at the surface) about 37 km (20 n mi) south of High Island, Texas around 0400 UTC 13 September, qualifying it as one of the most rapidly intensifying North Atlantic TCs (Brennan et al. 2007). After landfall, the hurricane moved northeastward toward southwestern Louisiana and became a tropical depression near Alexandria, Louisiana (late on 13 September) before it dissipated over Central Mississippi.

(ii) Hurricane Isaac (2012)

Unlike Hurricane Humberto of 2007, Hurricane Isaac originated from a tropical wave off the coast of West Africa and traversed across the Atlantic through the Caribbean region and the Gulf of Mexico before making landfall in southeastern Louisiana as a Category 1 hurricane. Isaac became a hurricane around 1200 UTC on 28 August, 2012 centered around 75 n mi southwest of the mouth of the Mississippi River. Isaac made the first landfall at Southwest Pass, Louisiana around 0000 UTC 29 August with maximum sustained winds of 70 kt. The center of the hurricane wobbled westward back over water and made a second landfall at Port Fourchon, Louisiana around 0800 UTC 29 August (Berg 2013). After landfall, the hurricane gradually weakened to a tropical depression around 0000 UTC 31 August in southern Arkansas as it steered northwestward across Louisiana (Fig. 4b). The depression finally dissipated around 0600 UTC on 1 September west-southwest of Jefferson City, Missouri (Fig. 4b). The remnants of Isaac produced several tornadoes across Mississippi River Valley on 1 September as it moved northeastward and eastward across Missouri and Illinois.

(iii) Hurricane Matthew (2016)

Like Hurricane Isaac, Hurricane Matthew originated from a tropical wave off the West African coast. It was one of the deadliest hurricanes that made multiple landfalls as a Category 5 hurricane along the coasts of Haiti, Cuba, Grand Bahama Island and as a Category 1 hurricane along the central coast of South Carolina, accounting for 585 deaths (Stewart 2017). Hurricane

Matthew remained about 30 n mi offshore of the Florida Atlantic coast, as a Category 2 hurricane with its winds hitting Cape Canaveral, Vero Beach and Jacksonville Beach in Florida by 0000 UTC 8 October 2016 (Fig. 4c). Hurricane Matthew continued to move northward towards South Carolina making landfall at 1500 UTC on 8 October at Cape Romain National Wildlife Refuge (Fig. 4c). As a result of the expanded hurricane forced wind field of this hurricane and its track along the eastern coast of southeastern United States, there was significant inundation from storm surge along the coasts and well inland of the coast of Florida, Georgia, and South Carolina (Stewart 2017).

(iv) Hurricane Harvey (2017)

Although, Hurricane Harvey also initiated from tropical wave off the coast of West Africa, it dissipated for a good part of its translation across the Caribbean Sea before it began to reform into a tropical depression in the Bay of Campeche by 1200 UTC of 23rd August 2017. Thereafter, it rapidly intensified in an environment of light shear, very warm water, and high mid-level moisture to a hurricane by 24 August and intensified to Category 4 hurricane by 0000 UTC 26 August 2017 (Blake and Zelinsky 2018). Harvey made landfall on Texas mainland 0600 UTC 26 August along the coast of Copano Bay and rapidly weakened to a tropical storm within 12 hours of the landfall. But Harvey remained nearly stationary with its center over or near the Texas coast for four days before it made its final landfall over southwestern Louisiana at 0800 UTC 30 August near Cameron (Fig. 4d). In this period of four days, it produced over 60 inches of rainfall over southeastern coast of Texas, causing catastrophic flooding.

S4: The evolution of the flash droughts associated with landfalling Atlantic tropical cyclone

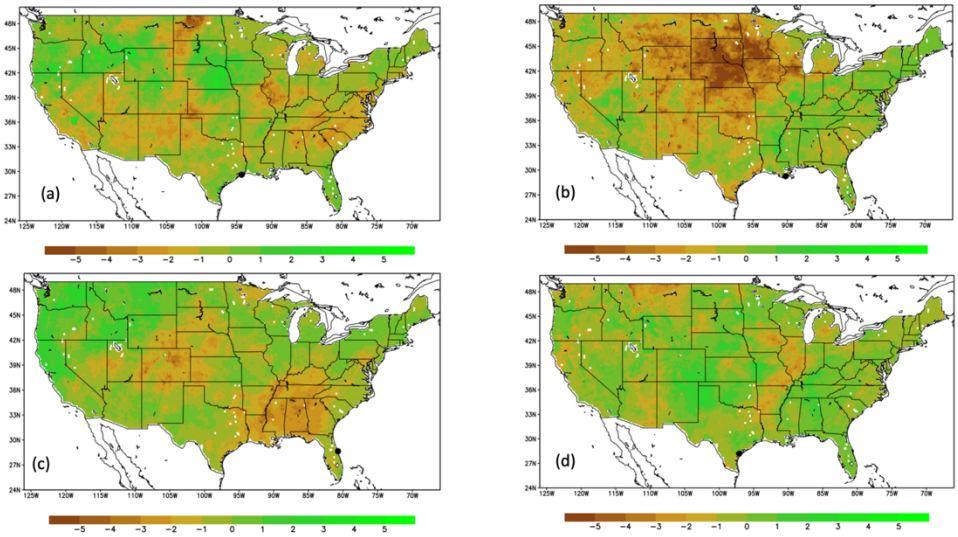

Figure FS5: The map of the normalized, daily cumulative anomalies of the soil moisture for the flash drought events associated with the landfall of Hurricanes a) Humberto of 2007, b) Isaac of 2012, c) Matthew of 2016, and d) Harvey of 2017. The daily normalized anomalies of the soil moisture are summed over the period of the flash drought as indicated in Figure 3. The black dot in each of the panels indicate the location of the landfall of the hurricane.

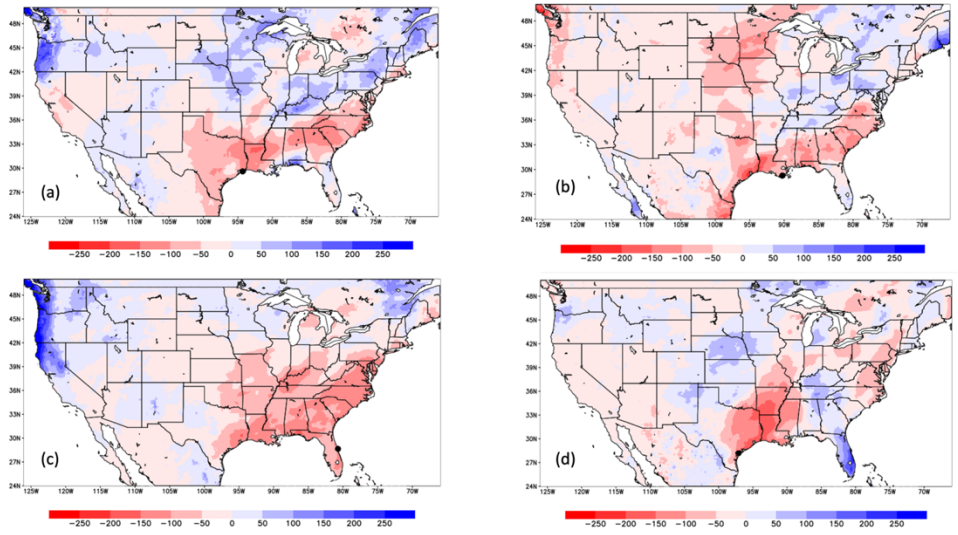

Figure FS6: The map of the normalized, daily cumulative anomalies of the precipitation for the flash drought events associated with the landfall of Hurricanes a) Humberto of 2007, b) Isaac of 2012, c) Matthew of 2016, and d) Harvey of 2017. The daily normalized anomalies of the surface temperature are summed over the period of the flash drought as indicated in Figure 3. The black dot in each of the panels indicate the location of the landfall of the hurricane.

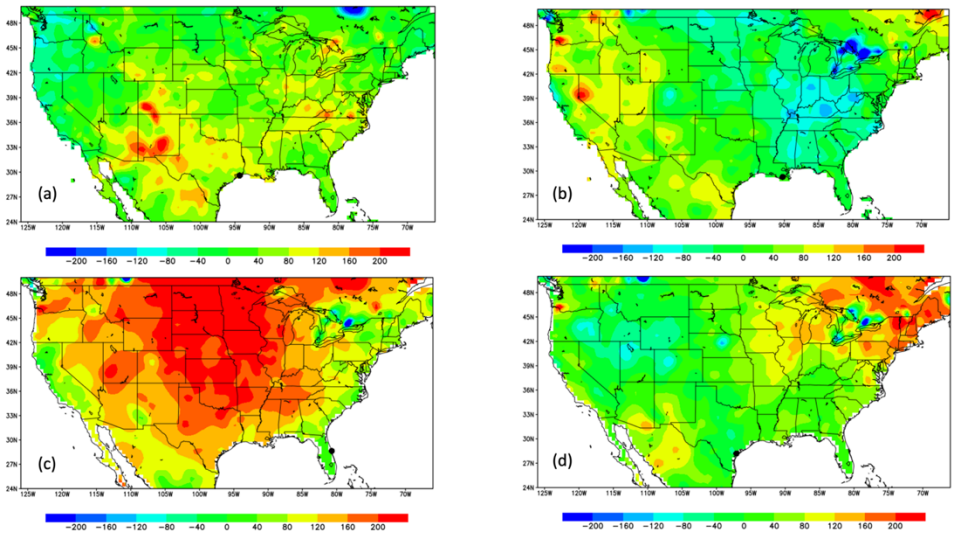

Figure FS7: The map of the normalized, daily cumulative anomalies of the surface temperature for the flash drought events associated with the landfall of Hurricanes a) Humberto of 2007, b) Isaac of 2012, c) Matthew of 2016, and d) Harvey of 2017. The daily normalized anomalies of the precipitation are summed over the period of the flash drought as indicated in Figure 3. The black dot in each of the panels indicate the location of the landfall of the hurricane.